Analysis of the Influence of Different Cycling Methods on the Structural Stress of Bicycles Based on Abaqus

Zhang Baiming, 3230100298

2025 年 6 月 29 日

1 Purpose and Scope

In today's society, bicycles serve as a convenient and environmentally friendly mode of transportation, playing a significant role in daily commuting and recreational activities. The stability and safety of their structure are paramount for the experience and well-being of cyclists. However, different cycling methods can exert varying impacts on the bicycle's structure, thereby influencing its performance and lifespan. Therefore, conducting an in-depth investigation into the effects of different cycling methods on the structure of bicycles holds great practical significance.

This project focuses on two typical cycling methods: coasting downhill without pedaling and cycling on a flat road. These methods are common in actual cycling scenarios and lead to significant differences in the stress conditions of the bicycle's structure. By utilizing the advanced Abaqus software for analysis and constructing a two-dimensional structural model to simplify the problem, we aim to thoroughly explore the impacts of these two cycling methods on the bicycle's structure, particularly the locations of maximum tensile stress and overall stress. Moreover, this project proposes an effective method to reduce the maximum tensile stress by 30%, in the hope of providing a scientific basis for the design and optimization of bicycles.

Despite the limitations of time and capability, which necessitated some simplifying assumptions during the research process, such as not accounting for the interactions among other bicycle components, the effects of dynamic loads, or real-world usage factors like wind resistance and road conditions, and assuming the material's mechanical properties to be linearly elastic, we believe that the research findings of this project can still offer valuable references for the optimized design of bicycle structures and lay a foundation for more in-depth future studies.

2 Model Simplification and Parameter Settings

I first retrieved the model diagram of the bicycle from the internet[1](shown as Fig.1). The diagram illustrates the basic structure of the bicycle, including the frame, wheels, handlebars, and seat.

[1]The picture cites from `https://www.lazystones.com/project/284331`

Fig.1 The model diagram of the bicycle

The frame, as the core supporting structure, connects the various components and is crucial for bearing and transferring loads. Given the frame's vital role as the core supporting structure that connects various components and bears and transfers loads, I am currently focusing on this part. The frame is roughly composed of seven rods, which I have simplified into the model shown in the following figure.

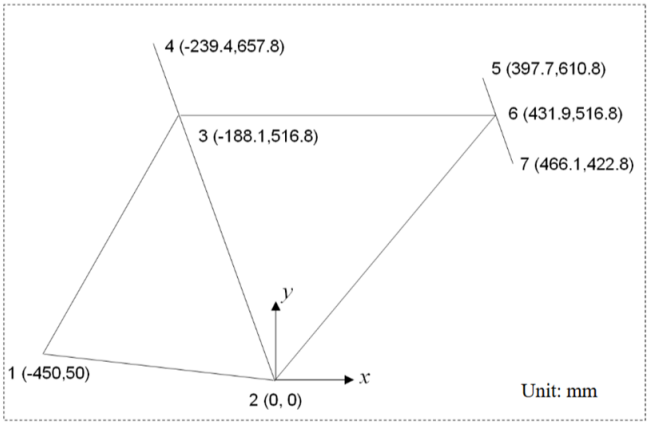

Fig.2: Bicycle's Frame Construction

We assume that all frame pipes are ideal cylindrical structures to ensure the simplicity and consistency of the analysis. The material is 6061T6 Aluminum Alloy with Young' s modulus 68.9 GPa and Poisson' s ratio 0.3.

Bar	**Outer Diameter (mm)**	**Wall Thickness (mm)**
1-2	30	3
1-3	30	3
2-3	35	3.5
Others	42	3.5

List.1: Dimensions of Bars

Loading Cases: We take two load cases into consider. The first load case includes only the vertical loads associated with the weight of the rider. The second load case involves the rider

applying a force on one pedal. This load case represents the maximum force the rider might apply to the drive train when pedaling.

Load Case	**Displacement Constraints**	**Applied Forces at each Point**
1	Point 1: $u_x = 0, u_y = 0$ Point 6: $u_y = 0$	Point 4: $F_y = -900$ N Point 5: $F_x = -120$ N Point 7: $F_x = 120$ N
2	Point 1: $u_x = 0, u_y = 0$ Point 6: $u_y = 0$	Point 2: $F_y = -600$ N Point 4: $F_y = -300$ N Point 5: $F_x = -120$ N Point 7: $F_x = 120$ N

List 2: Load Cases with Displacement Constraints and Applied Forces

3 Theoretical foundation

3.1 Describe an element

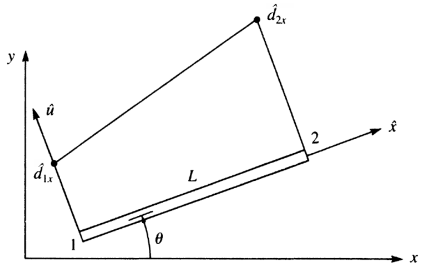

Fig.3: Displacement u plotted over the length of the element

Represent the bar by labeling nodes at each end and in general by labeling the element number.

Assume a linear displacement variation along the $\hat{x}$ axis of the bar because a linear function with specified endpoints has a unique path.

$$\hat{u} = [N_1 \quad N_2] \begin{Bmatrix} \hat{d}_{1x} \\ \hat{d}_{2x} \end{Bmatrix} = [\mathbf{N}]\{\boldsymbol{u}\} \tag{1}$$

with shape functions given by

$$N_1 = 1 - \frac{\hat{x}}{L} \quad N_2 = \frac{\hat{x}}{L} \tag{2}$$

Strain Calculation:

$$\varepsilon_x = \frac{du(x)}{dx} = \frac{d}{dx}([\mathbf{N}]\{\boldsymbol{u}\}) = \frac{d}{dx}([\mathbf{N}])\{\boldsymbol{u}\} = [\mathbf{B}]\{\boldsymbol{u}\} \tag{3}$$

In which:

$$[\mathbf{B}] = \frac{d}{dx}\left([N_i(x) \quad N_j(x)]\right) = \begin{bmatrix} -1/L & 1/L \end{bmatrix} \tag{4}$$

Stress Calculation:

$$\sigma_x = E\varepsilon_x = E[\mathbf{B}]\{\boldsymbol{u}\} = [\mathbf{D}][\mathbf{B}]\{\boldsymbol{u}\} \tag{5}$$

3.2 Total energy

Total potential energy is defined as the sum of the internal strain energy U and the potential energy of the external forces Ω; that is,

$$\pi_p = U + \Omega \tag{6}$$

Strain energy is the capacity of internal forces (or stresses) to do work through deformations (strains) in the structure; Ω is the capacity of forces such as body forces, surface traction forces, and applied nodal forces to do work through deformation of the structure.

For the bar element the *strain energy* is:

$$U(u) = \frac{1}{2}\iiint_V \sigma_x \varepsilon_x dV = \frac{A}{2}\int_0^L \sigma_x^T \varepsilon_x dx \tag{7}$$

$$= \frac{A}{2}\int_0^L \{\boldsymbol{u}\}^T[\mathbf{B}]^T[\mathbf{D}][\mathbf{B}]\{\boldsymbol{u}\}dx = \frac{AL}{2}\{\boldsymbol{u}\}^T[\mathbf{B}]^T[\mathbf{D}][\mathbf{B}]\{\boldsymbol{u}\} \tag{8}$$

For a bar element, none of these is a function of x.

The work potential (ignore the body force term) can be described as following:

$$\Omega = -\left(f_i u_i + f_j u_j\right) - \iint_{S_i} \boldsymbol{u}_s^T \boldsymbol{T}_x dS \tag{9}$$

$$= -\{\boldsymbol{u}\}^T\{\boldsymbol{P}\} - \iint_{S_i} \{\boldsymbol{u}\}^T[\boldsymbol{N}_s]^T\boldsymbol{T}_x dS \tag{10}$$

$$= -\{\boldsymbol{u}\}^T\{\boldsymbol{f}\} \tag{11}$$

In which: $\{\boldsymbol{f}\} = \{\boldsymbol{P}\} + \iint_{S_i}[\boldsymbol{N}_s]^T\boldsymbol{T}_x dS$

3.3 The stiffness matrix derived using the principle of minimum energy

To apply the principle of minimum potential energy—that is, to minimize π_p—we take the *variation* of π_p, which is a function of nodal displacements d_i defined in general as

$$\delta\pi_p = \frac{\partial \pi_p}{\partial d_1}\delta d_1 + \frac{\partial \pi_p}{\partial d_2}\delta d_2 + \cdots + \frac{\partial \pi_p}{\partial d_n}\delta d_n = 0 \tag{12}$$

The total potential energy is given by:

$$\Pi_p = \frac{AL}{2}\{\boldsymbol{u}\}^T[\mathbf{B}]^T[\mathbf{D}]^T[\mathbf{B}]\{\boldsymbol{u}\} - \{\boldsymbol{u}\}^T\{\boldsymbol{f}\} \tag{13}$$

The variation of the total potential energy leads to the equilibrium equation:

$$\frac{\delta\Pi_p}{\delta\{\boldsymbol{u}\}} = 0 \quad \Rightarrow \quad AL[\mathbf{B}]^T[\mathbf{D}]^T[\mathbf{B}]\{\boldsymbol{u}\} = \{\boldsymbol{f}\} \quad \Rightarrow \quad [\mathbf{k}]\{\boldsymbol{u}\} = \{\boldsymbol{f}\} \tag{14}$$

The matrices $[\mathbf{B}]$ and $[\mathbf{D}]$ are defined as:

$$[\mathbf{B}] = \begin{bmatrix} -1/L & 1/L \end{bmatrix} \quad [\mathbf{D}] = E \quad \{\boldsymbol{f}\} = \begin{Bmatrix} f_i \\ f_j \end{Bmatrix} \tag{15}$$

The final expression for the stiffness matrix is derived as:

$$[\mathbf{k}] = AL\begin{Bmatrix} -1/L \\ 1/L \end{Bmatrix} E \begin{bmatrix} -1/L & 1/L \end{bmatrix} = \frac{EA}{L}\begin{bmatrix} 1 & -1 \\ -1 & 1 \end{bmatrix} \tag{16}$$

3.4 Coordinate System Transformation in Beam Elements

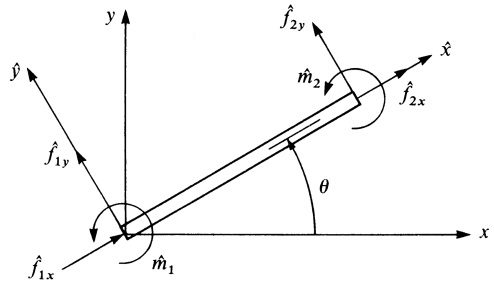

Fig.4: Local forces acting on a beam element

Unfortunately, our coordinates won't always strictly align along the x-axis, so we need to use a rotated coordinate system to handle two-dimensional beams. This is achieved using a transformation matrix **T**.

$$\begin{Bmatrix} u_i' \\ v_i' \\ \theta_i' \\ u_j' \\ v_j' \\ \theta_j' \end{Bmatrix} = \begin{bmatrix} C & S & 0 & 0 & 0 & 0 \\ -S & C & 0 & 0 & 0 & 0 \\ 0 & 0 & 1 & 0 & 0 & 0 \\ 0 & 0 & 0 & C & S & 0 \\ 0 & 0 & 0 & -S & C & 0 \\ 0 & 0 & 0 & 0 & 0 & 1 \end{bmatrix} \begin{Bmatrix} u_i \\ v_i \\ \theta_i \\ u_j \\ v_j \\ \theta_j \end{Bmatrix} \tag{17}$$

or

$$\mathbf{u}' = \mathbf{T}\mathbf{u} \tag{18}$$

The force vector **f** in the original coordinate system is transformed to the new coordinate system:

$$\mathbf{k}'\mathbf{u}' = \mathbf{f}' = \mathbf{T}\mathbf{f} = \mathbf{T}\mathbf{k}\mathbf{u} \tag{19}$$

From this, we can derive the stiffness matrix in the original coordinate system:

$$\mathbf{k} = \mathbf{T}^T\mathbf{k}'\mathbf{T} \tag{20}$$

Then we have the general transformed global stiffness matrix for a beam element that includes axial force, shear force, and bending moment effects as follows:

$$k = \frac{E}{L}\begin{bmatrix} AC^2 + \frac{12I}{L^2}S^2 & \left(A - \frac{12I}{L^2}\right)CS & -\frac{6I}{L}S & -\left(AC^2 + \frac{12I}{L^2}S^2\right) & -\left(A - \frac{12I}{L^2}\right)CS & -\frac{6I}{L}S \\ \left(A - \frac{12I}{L^2}\right)CS & AS^2 + \frac{12I}{L^2}C^2 & \frac{6I}{L}C & -\left(A - \frac{12I}{L^2}\right)CS & -\left(AS^2 + \frac{12I}{L^2}C^2\right) & \frac{6I}{L}C \\ -\frac{6I}{L}S & \frac{6I}{L}C & 4I & \frac{6I}{L}S & -\frac{6I}{L}C & 2I \\ -\left(AC^2 + \frac{12I}{L^2}S^2\right) & -\left(A - \frac{12I}{L^2}\right)CS & \frac{6I}{L}S & AC^2 + \frac{12I}{L^2}S^2 & \left(A - \frac{12I}{L^2}\right)CS & \frac{6I}{L}S \\ -\left(A - \frac{12I}{L^2}\right)CS & -\left(AS^2 + \frac{12I}{L^2}C^2\right) & -\frac{6I}{L}C & \left(A - \frac{12I}{L^2}\right)CS & AS^2 + \frac{12I}{L^2}C^2 & -\frac{6I}{L}C \\ -\frac{6I}{L}S & \frac{6I}{L}C & 2I & \frac{6I}{L}S & -\frac{6I}{L}C & 4I \end{bmatrix}$$

In which C means cosθ, and S means sinθ.

Then we have the equivalent Hooke's law between two nodes as follow:

$$\begin{Bmatrix} \hat{f}_{1x} \\ \hat{f}_{1y} \\ \hat{m}_1 \\ \hat{f}_{2x} \\ \hat{f}_{2y} \\ \hat{m}_2 \end{Bmatrix} = [k] \begin{Bmatrix} \hat{d}_{1x} \\ \hat{d}_{1y} \\ \hat{\phi}_1 \\ \hat{d}_{2x} \\ \hat{d}_{2y} \\ \hat{\phi}_2 \end{Bmatrix}$$

We have formulated the stiffness matrices for the seven bars, which are then assembled into a 21*21 global stiffness matrix. Subsequently, we can use the previously established stress-strain relationships to solve for the response of the entire structure. Given the complexity of the subsequent theoretical calculations, we have decided to entrust them to specialized simulation software.

4 Simulation using ABAQUS

4.1 When the rider rides without stepping the pedal

When the rider rides without stepping the pedal, the force given to the bycicle is shown as Fig.5.

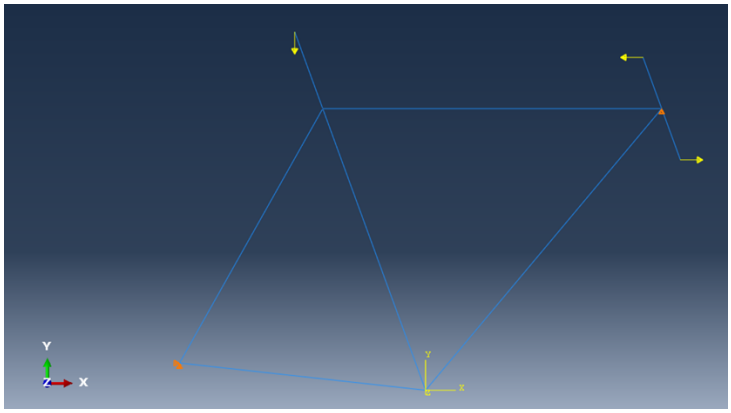

Fig.5: Force Distribution on Bicycle When Riding Without Pedaling

The maximum tensile stress occurs at the junction of node 3, as is shown in the Fig.6. The maximum stress value is 8.491.

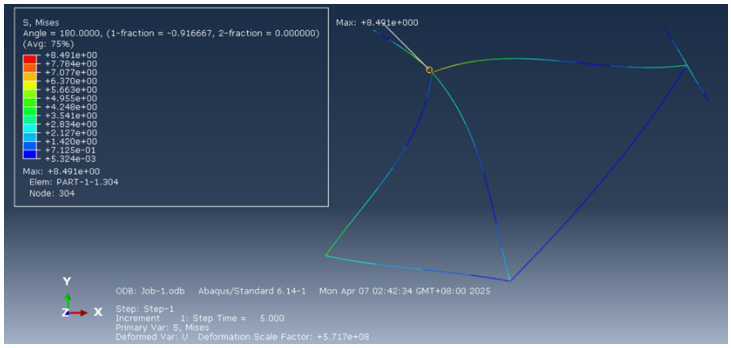

Fig.6: Distribution of Tensile Stress

The visualization of Fig.7 likely shows the rod's structure and the distribution of stress across it, with colors or other indicators representing varying degrees of deformation.

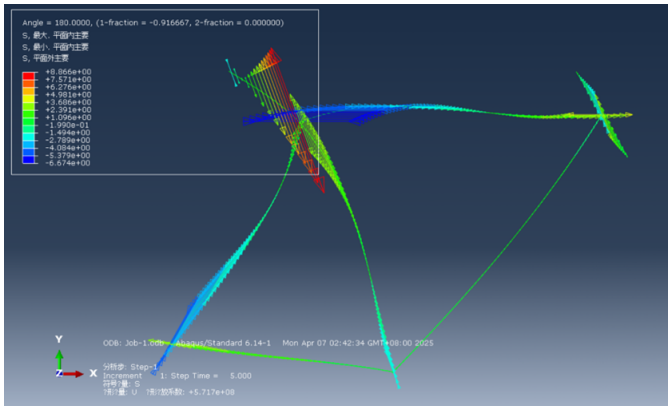

Fig.7: Deformation of Rod at Various Stress Levels

4.2 When the rider rides while stepping the pedal

When the rider rides while stepping the pedal, the force given to the bycicle is shown as Fig.8.

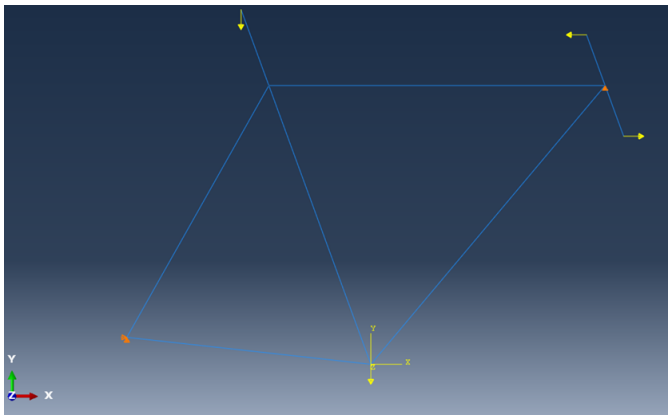

Fig.8: Force Distribution on Bicycle When Riding Without Pedaling

The maximum tensile stress occurs at the junction of node 3, as is shown in the Fig.9. The maximum stress value is 3.305.

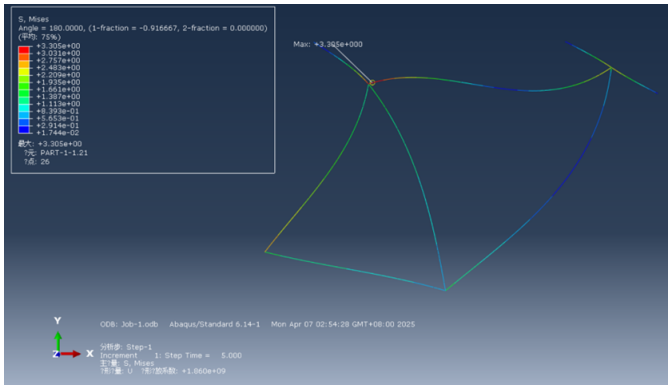

Fig.9: Distribution of Tensile Stress

The visualization of Fig.10 likely shows the rod's structure and the distribution of stress across it, with colors or other indicators representing varying degrees of deformation.

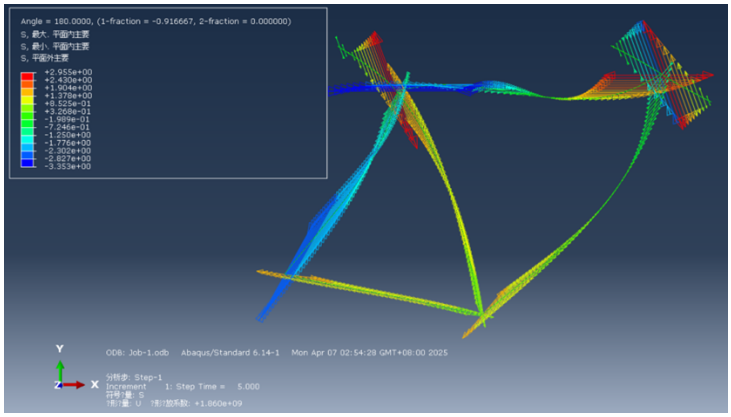

Fig.10: Deformation of Rod at Various Stress Levels

4.3 Reduce the maximum tensile stress by 30%

To achieve a reduction in the maximum tensile stress by 30%, several strategies can be implemented. Firstly, selecting a material with a greater Young's modulus will inherently increase the stiffness of the bar, thereby reducing the stress experienced under the same load conditions.

Additionally, modifying the geometry of the bar can also be effective. By altering the outer diameter and wall thickness, we can significantly change the cross-sectional moment of inertia, which is a crucial factor in determining the bar's resistance to bending and torsional stresses. Specifically, increasing the moment of inertia can lead to a more robust structure that can better withstand applied loads.

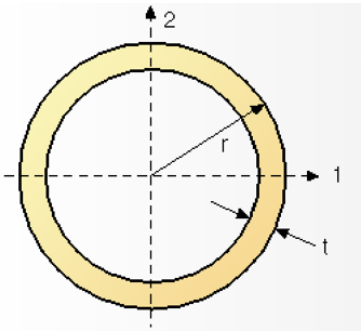

Fig.11: Ring's cross-section

For the ring's cross-section moment of inertia, the formula is

$$I_z = \frac{\pi}{4}(R^4 - r^4)$$

where R is the outer radius and r is the inner radius. To reduce the maximum tensile stress while using the same amount of material, we can list

$$\begin{cases} \frac{R}{\frac{\pi}{4}(R^4 - r^4)} \times (1 - 30\%) = \frac{R_*}{\frac{\pi}{4}(R_*^4 - r_*^4)} \\ \pi(R^2 - r^2) = \pi(R_*^2 - r_*^2) \end{cases}$$

For instance, consider transforming a hollow cylinder with an outer radius $R = 21$ mm and an inner radius $r = 17.5$ mm into one with an outer radius $R_* = 27.837$ mm and an inner radius $r_* = 25.301$ mm. This modification not only increases the cross-sectional area but also enhances the moment of inertia, thereby reducing the maximum tensile stress by distributing the load more effectively across the structure.

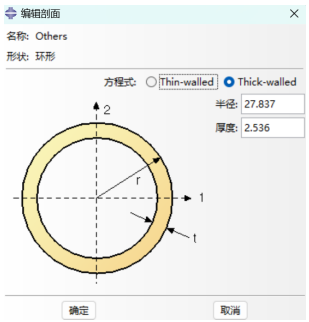

Fig.12: Optimized radius

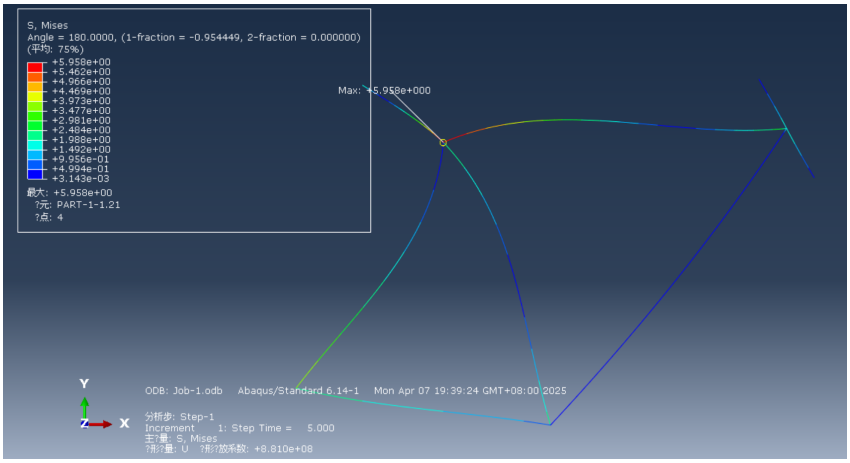

Fig.13: Maximum tensile stress after optimizing the radius

As we can see in Fig.13, the maximum tensile stress deduced from 8.491 to 5.958, with the decreasing rate of exactly $(8.491-5.958)/8.491*100\% \approx 30\%$. This result also proves the rationality of the theory in the reverse way.

5 Conclusions and Recommendations

This report has successfully identified the critical locations within the bicycle structure where maximum tensile stress occurs. By conducting a thorough analysis, we have pinpointed the areas subjected to the highest stress levels, which are crucial for ensuring the safety and longevity of the bicycle. Furthermore, we have developed an effective method to reduce the maximum tensile stress by 30%. This reduction is achieved through a combination of strategic material selection and structural optimization techniques.

Despite the limitations in the conditions considered and the presence of certain defects in our analysis, such as not accounting for the interactions among other bicycle components, the effects

of dynamic loads, or real-world usage factors like wind resistance and road conditions, the findings of this report hold significant reference value. The assumptions made, including the linear elastic behavior of the material, while simplifying the analysis, provide a robust foundation for further studies.

The recommendations provided in this report can serve as a guide for bicycle design and manufacturing, potentially leading to improvements in the structural integrity and performance of bicycles. By implementing these strategies, manufacturers can enhance the durability and safety of their products, thereby increasing consumer confidence and satisfaction.

For future research, it is recommended to expand the analysis to include more realistic loading conditions and material behaviors. Incorporating non-linear material properties and multi-axial loading scenarios could provide a more comprehensive understanding of the structural response under various cycling conditions. Additionally, exploring advanced materials and innovative design methodologies could further optimize the bicycle's performance and resilience.

In conclusion, this study has provided valuable insights into the structural stress distribution of bicycles under different cycling methods and has offered practical solutions to mitigate stress concentrations. The findings and recommendations presented herein can significantly contribute to the development of more robust and reliable bicycle designs.